QUARTERLY OF APPLIED MATHEMATICS VOLUME LXXIX, NUMBER 4 DECEMBER 2021, PAGES 695–715 https://doi.org/10.1090/qam/1598 Article electronically published on July 9, 2021

MODELS OF BACTERIA SWIMMING IN A NEMATIC LIQUID CRYSTAL

Ву

MOCHONG DUAN (Department of Mathematical Sciences, Carnegie Mellon University, Pittsburgh, Pennsylvania 15213)

AND

NOEL J. WALKINGTON (Department of Mathematical Sciences, Carnegie Mellon University, Pittsburgh, Pennsylvania 15213)

Abstract. Models of dilute systems of bacteria swimming in a nematic liquid crystal are developed and analyzed. The motion and orientation of the bacteria are simulated using ordinary differential equations coupled with the partial differential equations modeling the nematic liquid crystal (Ericksen Leslie equations). The analysis and numerical simulations of this system are shown to predict interesting phenomena observed experimentally.

1. Introduction. This work is motivated by the experimental observation that, in certain configurations, the motion of bacteria swimming in a nematic liquid crystal is strongly influenced by the nematic configuration [11]. In these experiments bacteria were swimming in a liquid crystal medium "sandwiched" between glass plates coated with a spiral pattern as illustrated in Figure 1.2. Since the nematic configuration of liquid crystals can be controlled through boundary conditions and electric fields, and swimming activity by oxygen concentration, this offers the possibility of controlling bacteria transport.

The concentration of bacteria in the experiments in [11] was low enough to record the motion of individual bacteria; Figure 1.1 illustrates this¹. In this dilute limit we model the experimental configuration as a finite number of active particles in a nematic liquid crystal. The model presented below is an extension of the one presented in [8], and much of the analysis presented below extends directly to the latter. While the

Received March 2, 2021, and, in revised form, April 27, 2021.

2020 Mathematics Subject Classification. Primary 92-10, 37M25, 35Q92.

Key words and phrases. Swimming, bacteria, liquid crystal.

The second author was supported in part by National Science Foundation Grants DREF-1729478 and DMS-2012259. This work was also supported by the NSF through the Center for Nonlinear Analysis. *Email address*: mduan@andrew.cmu.edu

 $Email\ address:$ noelw@andrew.cmu.edu

¹The authors thank O. Lavrentovich and R. Koizumi of the Liquid Crystal Institute at Kent State University for images of their experiments and permission to reproduce them.

©2021 Brown University



Fig. 1.1. Trajectories of bacteria swimming in a nematic liquid crystal.

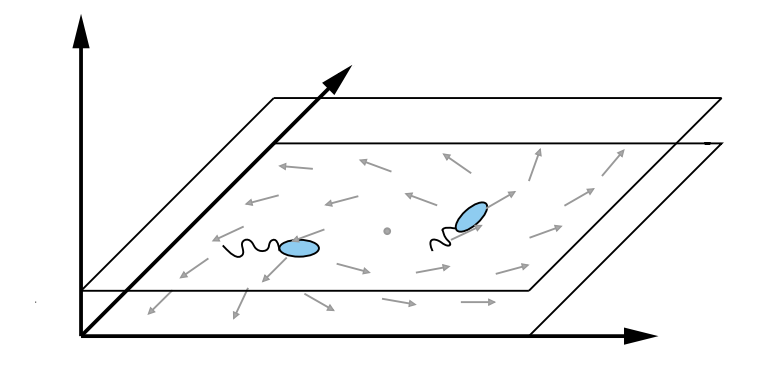


Fig. 1.2. Experimental configuration.

equations modeling this system hold in both two and three dimensions, we focus on the two dimensional configuration illustrated in Figure 1.2 where the region between the glass plates is thin. The inner surfaces of the glass plates are coated with organic dye molecules that are photoaligned to form a spiral pattern [16]. Surface anchoring and elasticity of the nematic filling the space between the glass plates causes the nematic director to follow the patterned spirals. A detailed description of the experimental configuration can be found in [11, 26, 27]

When the boundary conditions in the third dimension dominate, the fluid velocity is negligible and the nematic orientation is fixed. In this situation the motion of the bacteria is modeled by a pair of ODE's for their position and orientation. In Section 2 we show that solutions of these ODE's can exhibit some of the richness of properties reported in the experiments. For various spiral configurations and initial conditions, solutions with circular orbits are shown to exist and their stability is investigated. In Section 3 the dynamics for swimming particles is coupled with the Ericksen Leslie equations which model the hydrodynamics of a nematic liquid crystal. Weak statements of the coupled system are formulated for which Galerkin (numerical) approximations inherit the natural energy estimates. Numerical simulations are presented in Section 5 to illustrate the properties of the solutions and comparison with experimental results and other approaches is considered.

- 1.1. Models of swimming. There is a large body of work focusing on mathematical modeling of swimming. Essentially all of this work considers the fluid medium to be a Newtonian fluid which is typically incompressible. For small swimmers, such as bacteria, the inertial forces are negligible and the motion of a Newtonian fluid is governed by linear (Stokes') equations. In this situation the models can generally be classified according to the length scale being resolved.
 - At the finest length scale, the geometry of the swimmer is parameterized and deformations which result in net motion are investigated [1,4,5]. In these models the Dirichlet–to–Neumann map for Stokes' equations is used on the boundary to determine the traction due to the fluid.
 - Mesoscale models utilize a Boltzman approach with Jeffery's ODE's [2, 10] for the motion of an ellipsoid in a Newtonian fluid modeling the particle kinematics. The particle density is then transported (pushed forward) by the corresponding flow [3, 18]. The density is defined on the phase space which is high dimensional (position and velocity), so closure models are required to render the problem computationally tractable.
 - Macroscopic models typically represent the particle kinematics as a diffusion due to the swimming action superimposed upon a drift given by the underlying fluid velocity. The balance of mass then gives an equation for the concentration of the bacteria. The momentum equation for the fluid is then augmented with an additional stress to simulate the momentum transfer due to the swimming action [13,15,20–22,25].

In addition to the usual viscous stresses, nematic fluids also support elastic stresses which renders their equations of motion intrinsically nonlinear. In this situation Green's function techniques are not available; in particular, analogs of Jeffery's equations for the motion of ellipsoids in a liquid crystal are not available [24].

2. Modeling bacterial motion. In this section we develop a system of ODE's to model the position and orientation a particles in a nematic liquid crystal under the influence of a propulsive force, as illustrated in Figure 1.3.

ASSUMPTION 2.1. Let $\mathbf{y}(t)$ and $\mathbf{m}(t)$, with $|\mathbf{m}(t)| = 1$, denote the position and orientation of a bacterium in a nematic liquid crystal with velocity and director fields $(\mathbf{v}(t,x),\mathbf{n}(t,x))$. Typically $|\mathbf{n}| \simeq 1$; however, this can not hold near singularities.

(1) The concentration of bacteria is sufficiently low so that the interaction of the bacteria with each other is mediated through the liquid crystal medium.

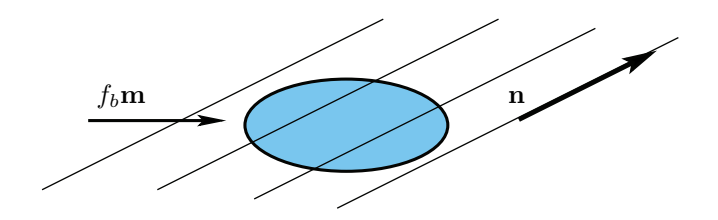


Fig. 1.3. Particle in a nematic with a body force.

- (2) Viscous and elastic forces on the bacteria dominate the inertial forces, so the latter can be neglected.
- (3) Translation and rotation of the bacterial give rise to viscous dissipation of the form

$$\mathcal{R}_b = (c_t/2)|\dot{\mathbf{y}}(t) - \mathbf{v}(t,\mathbf{y}(t))|^2 + (c_r/2)|\dot{\mathbf{m}}(t) - W\left(\mathbf{v}(t,\mathbf{y}(t))\right)\mathbf{m}(t)|^2,$$

where $W(\mathbf{v}) = (1/2) (\nabla \mathbf{v} - (\nabla \mathbf{v})^{\top})$, and $c_t, c_r > 0$ are viscous coefficients.

(4) The elastic energy due to local alignment of the nematic with the bacteria takes the form $W_b(\mathbf{m}(t), \mathbf{n}(t, \mathbf{y}(t)))$. Prototypically

$$W_b(\mathbf{m}, \mathbf{n}) = (k_b/2)|\mathbf{m} \times \mathbf{n}|^2 = (k_b/2)(|\mathbf{n}|^2 - (\mathbf{m} \cdot \mathbf{n})^2); \tag{2.1}$$

in particular, the elastic energy vanishes when the bacteria aligns with the nematic.

(5) The propulsive force due to the flagellum is of the form f_b **m**, where f_b is a constant. This constant may take either sign depending upon whether the bacteria is a "pusher" or "puller" [13]

To simplify the notation we write $\mathbf{v}(\mathbf{y})$ for $\mathbf{v}(t, \mathbf{y}(t))$ and $W(\mathbf{v}(\mathbf{y}))$ for the skew part of $\nabla \mathbf{v}(t, \mathbf{y}(t))$ when the context is clear.

Remark 2.2. The viscous dissipation and elastic energies in the above can be identified with the first order terms in any expansion of these quantities in the following sense.

• Viscous dissipation must depend upon differences (or gradients) of velocities and vanish when the velocities are zero. The motion of a short rigid rod in a shear flow [2, 10] is given by $\dot{\mathbf{y}} = \mathbf{v}$ and $\dot{\mathbf{m}} = W(\mathbf{v})\mathbf{m}$. Deviation from these relations gives rise to dissipation.

The ratio of length to diameter of the bacteria in [8,9,28] is O(10:1), so they are almost rod-like. If they were more elliptical (or disk shaped), the orientation would evolve according to an equation of the form $\dot{\mathbf{m}} = (a(\nabla \mathbf{v}) - b(\nabla \mathbf{v})^{\top})\mathbf{m}$ (assuming the fluid is incompressible).

• Independence of observer requires $W_b(Q\mathbf{m}, Q\mathbf{n}) = W_b(\mathbf{m}, \mathbf{n})$ for Q orthogonal, in which case $W_b(\mathbf{m}, \mathbf{n}) = \tilde{W}_b(|\mathbf{n}|, \mathbf{m}.\mathbf{n})$. Equation (2.1) is the first order term in an expansion of a non-negative energy which vanishes when the orientations align or $\mathbf{n} = 0$.

In the absence of inertia, Hamilton's principle for the motion of a particle states that for all times $t_1 < t_2$ and variations $(\mathbf{y}, \mathbf{m}) \mapsto (\mathbf{y} + \delta \mathbf{y}, \mathbf{m} + \delta \mathbf{m})$ with $\mathbf{m}.\delta \mathbf{m} = 0$ and compact support in (t_1, t_2) must satisfy

$$\delta \int_{t_1}^{t_2} W_b(\mathbf{m}, \mathbf{n}(\mathbf{y})) = \int_{t_1}^{t_2} \left\{ f_b \mathbf{m} \cdot \delta \mathbf{y} - \frac{\partial \mathcal{R}_b}{\partial \dot{\mathbf{y}}} \cdot \delta \mathbf{y} - \frac{\partial \mathcal{R}_b}{\partial \dot{\mathbf{m}}} \cdot \delta \mathbf{m} \right\}.$$

The variation of the elastic energy with respect to y is computed as

$$\delta_{\mathbf{y}} \mathcal{W}_b(\mathbf{m}, \mathbf{n}) = \frac{\partial \mathcal{W}_b}{\partial \mathbf{n}} . \delta_{\mathbf{y}} \mathbf{n}(\mathbf{y}) = \frac{\partial \mathcal{W}_b}{\partial \mathbf{n}} . (\nabla \mathbf{n}) \delta_{\mathbf{y}},$$

so that the equations of motion for a single bacteria take the form

$$c_t(\dot{\mathbf{y}} - \mathbf{v}) + (\nabla \mathbf{n})^{\top} \frac{\partial \mathcal{W}_b}{\partial \mathbf{n}} = f_b \mathbf{m}, \quad \text{and} \quad c_r(\dot{\mathbf{m}} - W(\mathbf{v}(\mathbf{y}))\mathbf{m}) + \frac{\partial \mathcal{W}_b}{\partial \mathbf{m}} + \lambda \mathbf{m} = 0, (2.2)$$

where λ is the Lagrange multiplier dual to the constraint $|\mathbf{m}| = 1$.

2.1. Spiral director with negligible hydrodynamics. In this section the experimental configuration in [11] is modeled as a two dimensional domain with planar bacteria orientation and liquid crystal director, and consider the situation where boundary conditions $(\mathbf{v}, \mathbf{n}) = (\mathbf{0}, \mathbf{n}_s(x))$ in the third dimension are sufficiently strong to render the disturbance of the nematic due to bacterial action negligible. Solutions of the equations (2.2) then satisfy

$$\frac{d\mathcal{W}_b}{dt} + c_t |\dot{\mathbf{y}}|^2 + c_r |\dot{\mathbf{m}}|^2 = f_b \mathbf{m}.\dot{\mathbf{y}}.$$

The experiments reported in [11] had a spiral pattern on the glass plates of the form

$$\mathbf{n}_s(x) = \frac{Rx}{\sqrt{|x|^2 + \epsilon}}, \quad \text{where} \quad R = \begin{bmatrix} \cos(\phi) & -\sin(\phi) \\ \sin(\phi) & \cos(\phi) \end{bmatrix}, \quad (2.3)$$

 $\phi \in [0, \pi/2]$ is the spiral angle, as in Figure 1.2, and the parameter $\epsilon \geq 0$ parameterizes the size of the "core" of the singularity.

In this situation it is possible to express equations (2.2) in polar coordinates. Letting

$$\mathbf{y}(t) = r(t) \left(\cos(\theta(t)), \sin(\theta(t)) \right), \quad \text{and} \quad \mathbf{m}(t) = \left(\cos(\psi(t)), \sin(\psi(t)) \right),$$

a calculation shows

$$c_{t}\dot{r} = f_{b}\cos(\psi - \theta) - \frac{k_{b}r}{(r^{2} + \epsilon)^{2}}\sin(\theta - \psi + \phi)^{2}\epsilon$$

$$c_{t}r\dot{\theta} = f_{b}\sin(\psi - \theta) - \frac{k_{b}r}{2(r^{2} + \epsilon)}\sin(2(\theta - \psi + \phi))$$

$$c_{r}\dot{\psi} = \frac{k_{b}r^{2}}{2(r^{2} + \epsilon)}\sin(2(\theta - \psi + \phi)).$$
(2.4)

when the elastic energy is given by equation (2.1).

This formulation of the equations is used to compute numerical solutions presented below. However, for their analysis it is convenient to consider a combination of angles which reduces the size of the system from three to two unknowns. Specifically, letting $\eta(t) = \theta(t) - \psi(t) + \phi$ gives the pair of equations for $(r(t), \eta(t))$,

$$\dot{r} = \frac{f_b}{c_t} \cos(\phi - \eta) - \frac{k_b r}{c_t (r^2 + \epsilon)^2} \sin(\eta)^2 \epsilon, \qquad (2.5)$$

$$\dot{\eta} = \frac{f_b}{c_t r} \sin(\phi - \eta) - \frac{k_b}{2(r^2 + \epsilon)} \left(\frac{1}{c_t} + \frac{r^2}{c_r}\right) \sin(2\eta).$$

2.2. Invariant region & long time behavior. We show that there is an invariant region of equations (2.5) in the (r, η) plane for which the radius of all solutions diverge to infinity (see Figure 2.1).

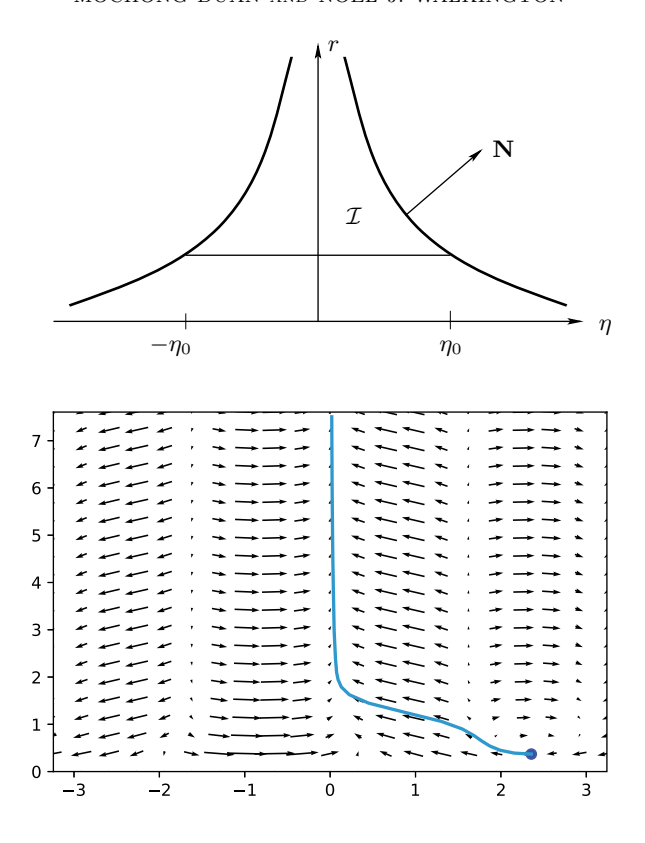


Fig. 2.1. Invariant region and plot of a solution in the (η, r) plane.

LEMMA 2.3. Let
$$\phi \in (-\pi/2, \pi/2)$$
 and $0 < \eta_0 < \pi/2 - |\phi|$ and $R(\eta) = K/\sin(\eta)$. Then
$$\mathcal{I} = \{(r, \eta) \mid |\eta| \le \eta_0, \ R(\eta_0) \le r \le R(\eta)\}, \tag{2.6}$$

is an invariant region of the differential equations (2.5) whenever

$$K \geq \max \left\{ \frac{c_r |f_b|}{c_t k_b} \left(\frac{\tan(\eta_0) + 1}{\cos(\eta_0)} \right) \left(\frac{R(\eta_0)^2}{R(\eta_0)^2 + \epsilon} \right), \left(\frac{k_b \sqrt{\epsilon}}{2c_t \cos(\pi/2 - |\phi|)} \right)^{1/2} \sin(\eta_0) \right\}.$$

If $(r, \eta) \in \mathcal{I}$ then $|\eta| \leq \eta_0$, and if $\epsilon = 0$,

$$\dot{r} = (f_b/c_t)\cos(\phi - \eta) \ge (f_b/c_t)\cos(\pi/2 - |\phi|) > 0$$
 so, $r(t) \to \infty$,

and since $R(|\eta|) \ge r$ for $(r, \eta) \in \mathcal{I}$,

$$\frac{K}{|\sin\big(\eta(t)\big)|} = R\left(|\eta(t)|\right) \ge r(t) \to \infty \qquad \text{ so, } \qquad \eta(t) \to 0.$$

Proof. Writing the differential equation (2.5) as $(\dot{r}, \dot{\eta}) = \mathbf{F}(r, \eta)$, it suffices to show that $\mathbf{F}(r, \eta).\mathbf{N}(r, \eta) \leq 0$ at each point $(r, \eta) \in \partial \mathcal{I}$, where $\mathbf{N}(r, \eta)$ denotes an outward normal to \mathcal{I} .

Write the boundary as the union of the bottom, left, and right hand sides,

$$\partial \mathcal{I} = R(\eta_0) \times (-\eta_0, \eta_0) \, \cup \, \{ (R(\eta), \eta) \mid \, \eta \in (0, \eta_0) \} \, \cup \, \{ (R(\eta), -\eta) \mid \, \eta \in (0, \eta_0) \}.$$

Bottom: The outward normal at the bottom is $\mathbf{N} = (-1,0)^{\mathsf{T}}$ so that

$$\mathbf{F}(\eta, r).\mathbf{N} = -\cos(\phi - \eta) + \frac{k_b}{c_t} \frac{R(\eta_0)\epsilon}{(R(\eta_0)^2 + \epsilon)^2} \sin(\eta)^2$$

$$\leq -\cos(\pi/2 - |\phi|) + \frac{k_b}{2c_t} \frac{\sqrt{\epsilon}}{(R(\eta_0)^2 + \epsilon)}$$

$$\leq -\cos(\pi/2 - |\phi|) + \frac{k_b}{2c_t} \frac{\sin(\eta_0)^2}{K^2} \sqrt{\epsilon}.$$

Left and Right Hand Sides: Since $\sin(\eta)$ is an odd function it suffices to consider the right hand side. At a boundary point $(R(\eta), \eta)$ with $\eta > 0$ an outward normal is

$$\mathbf{N}(\eta) = \begin{pmatrix} 1 \\ -R'(\eta) \end{pmatrix} = \begin{pmatrix} 1 \\ K\cos(\eta)/\sin^2(\eta) \end{pmatrix} = \begin{pmatrix} 1 \\ R(\eta)\cos(\eta)/\sin(\eta) \end{pmatrix}.$$

Writing $R = R(\eta)$ and $\mathbf{N} = \mathbf{N}(\eta)$ we have

$$F(\eta, R).\mathbf{N} = \frac{f_b}{c_t} \cos(\phi - \eta) - \frac{k_b R}{c_t (R^2 + \epsilon)^2} \sin(\eta)^2 \epsilon$$

$$\left(\frac{f_b}{c_t R} \sin(\phi - \eta) - \frac{k_b}{(R^2 + \epsilon)} \left(\frac{1}{c_t} + \frac{k_b R^2}{c_r}\right) \cos(\eta) \sin(\eta)\right) \frac{R \cos(\eta)}{\sin(\eta)}$$

$$\leq \frac{|f_b|}{c_t} + \left(\frac{|f_b|}{c_t} - \frac{k_b R^2}{c_r (R^2 + \epsilon)} \cos(\eta) K\right) \frac{\cos(\eta)}{\sin(\eta)}.$$

In the second step the cosine and sine of $\phi - \eta$ were bounded by unity, and the identity $R\sin(\eta) = K$ was used. Continuing,

$$F(\eta, R).\mathbf{N} \leq \frac{|f_b|}{c_t} \left(1 + \frac{\cos(\eta)}{\sin(\eta)} \right) - \frac{k_b R^2}{c_r (R^2 + \epsilon)} \frac{\cos^2(\eta)}{\sin(\eta)} K$$

$$= \frac{|f_b|}{c_t} \left(\frac{\sin(\eta)}{\cos(\eta)} + 1 - \frac{c_t k_b}{c_r |f_b|} \frac{R^2}{(R^2 + \epsilon)} \cos(\phi) K \right) \frac{\cos(\eta)}{\sin(\eta)}$$

$$\leq \frac{|f_b|}{c_t} \left(\tan(\eta_0) + 1 - \frac{c_t k_b}{c_r |f_b|} \frac{R(\eta_0)^2}{(R(\eta_0)^2 + \epsilon)} \cos(\eta_0) K \right) \frac{\cos(\eta)}{\sin(\eta)}$$

$$\leq 0,$$

where the last lines follows since $0 < \eta \le \eta_0 < \pi/2$ and K is sufficiently large. QED

- 2.3. Radial solution. Setting $\phi = 0$ gives the hedgehog director $\mathbf{n}_s(x) = x/\sqrt{|x|^2 + \epsilon}$, and $\dot{\eta}$ vanishes when $\sin(\eta) = 0$. Then $\theta = \psi$ or $\theta = \psi + \pi$ are constant so \mathbf{m} is parallel to \mathbf{y} and $r(t) = r(0) \pm f_b t$.
- 2.4. Circular trajectories. When $\epsilon=0$ explicit solutions of the stationary values of (2.5) are available. In this case $\dot{r}=0$ requires $\cos(\phi-\eta)=0$ so that $\eta(t)=\phi\pm\pi/2$ is constant. The equation for $\dot{\eta}=0$ then reduces to a quadratic equation for the radius,

$$\left(\frac{c_t}{c_r}\right)r^2 \pm \left(\frac{2f_b}{k_b\sin(2\phi)}\right)r + 1 = 0.$$

Selecting the sign so that the roots are non-negative gives solutions with circular trajectories at radii

$$r_{\pm} = \frac{c_r |f_b|}{c_t k_b \sin(2\phi)} \pm \sqrt{\left(\frac{c_r f_b}{c_t k_b \sin(2\phi)}\right)^2 - \frac{c_r}{c_t}}.$$

Then

$$\theta(t) = \theta(0) + \frac{1}{c_r r} \left(|f_b| - \frac{k_b}{2r} \sin(2\phi) \right) t$$
, and $\psi(t) = \psi(0) - \frac{k_b}{2c_r} \sin(2\phi) t$.

2.4.1. Stability. When $\epsilon=0$ the formula for the Jacobian of the right hand side of (2.5) is

$$\begin{bmatrix} \partial \dot{r}/\partial r & \partial \dot{r}/\partial \eta \\ \partial \dot{\eta}/\partial r & \partial \dot{\eta}/\partial \eta \end{bmatrix} = \begin{bmatrix} 0 & -\frac{f_b}{c_t} \\ \frac{1}{c_t r^2} (f_b - \frac{k_b \sin{(2\phi)}}{r}) & k_b \cos{(2\phi)} (\frac{1}{c_t r^2} + \frac{1}{c_r}) \end{bmatrix},$$

and the eigenvalues can be written as

$$\lambda = \frac{b \pm \sqrt{b^2 + c}}{2c_r c_t r^2}$$
, with $b = k_b \cos(2\phi)(c_t r^2 + c_r)$ and $c = 4c_r^2 f_b r(k_b \sin(2\phi) - f_b r)$,

The salient features of these expressions for the circular orbits with prototypical physical parameters are:

- b < 0 when $\phi > \pi/4$ and typically c < 0 for the larger radius and c > 0 for the smaller radius, so the former is stable and latter unstable.
- b > 0 when $\phi < \pi/4$, and solutions are unstable; prototypically $r(t) \to \infty$.
- b = 0 when $\phi = \pi/4$, and the sign of the expression under the radical is determined by $k_b f_b r$. For the larger radius $\pm \sqrt{c}$ are imaginary and the corresponding solution is marginally stable. For the smaller radius $\pm \sqrt{c}$ are real so this solution is unstable.
- 2.4.2. Finite core ($\epsilon > 0$). When $\epsilon > 0$ formulae for the roots of the stationary solutions of equations (2.5) are not available; however, for $0 < \epsilon << 1$ solution branches emanate from the two solutions with $\epsilon = 0$. In addition, a third solution may branch from r = 0 which is a singular point when $\epsilon = 0$.

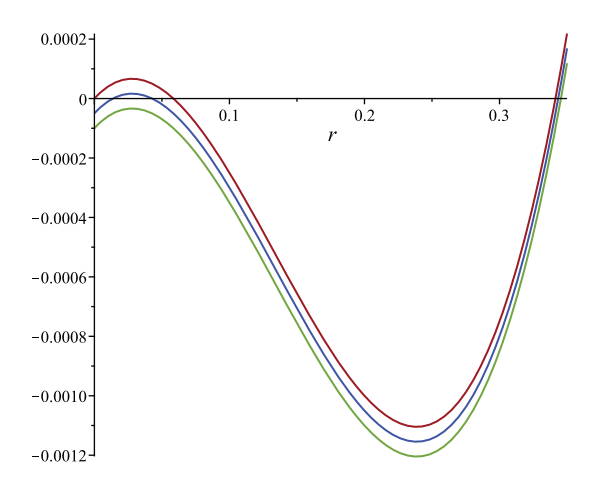


FIG. 2.2. Plots of $r(r^2 + \epsilon)\dot{\eta}$ with $\phi = \pi/4$, $\eta = 3\pi/4$ and $\epsilon \in \{0, 0.0005, 0.001\}$ (top, middle, bottom). Roots are radii of solutions with circular orbits.

EXAMPLE 2.4. If $\phi = \pi/4$ and $\eta = 3\pi/4$ the right hand side of $(2.5)_1$ vanishes. With ϵ fixed, roots of $(2.5)_2$ plotted as a function of r give the radii of the solutions with circular orbits.

This is illustrated in Figure 2.2 with $k_b = 0.1$, $f_b = 2$ $c_r = 0.25$ and $c_t = 20$. If $0 < \epsilon \lesssim 0.0007$ a third solution bifurcating from r = 0 is present. As ϵ increases this solution merges second solution when $\epsilon \simeq 0.0007$. For $\epsilon \gtrsim 0.0007$ only one solution exists. When $\epsilon = 0.1$, the radii for circular trajectories is 0.61, and in this case, the Jacobian of the right hand side of (2.5) has eigenvalues $0.0029 \pm 0.1887i$, and the small positive real part renders the corresponding solutions slightly unstable.

2.5. Constant speed model. Motivated by the experimental observation that there was very little variation in the speed of the bacteria, the following pair of equations was proposed in [11] to model their motion,

$$\dot{y} - \mathbf{v} = v_b \mathbf{m}, \quad \text{and} \quad c_r \left(\dot{\mathbf{m}} - W(\mathbf{v}(\mathbf{y})) \right) + \frac{\partial \mathcal{W}_b}{\partial \mathbf{m}} + \lambda \mathbf{m} = 0.$$

Here $v_b = f_b/c_t$ is the speed of the bacteria relative to the fluid, and is constant when the elastic forces are neglected.

With $\mathbf{v} = 0$ and the spiral director pattern and polar coordinates introduced in Section 2.1, these equations become

$$c_t \dot{r} = f_b \cos(\psi - \theta), \qquad c_t r \dot{\theta} = f_b \sin(\psi - \theta), \qquad c_r \dot{\psi} = \frac{k_b r^2}{2(r^2 + \epsilon)} \sin(2(\theta - \psi + \phi)).$$
 (2.7)

Setting $\eta = \theta - \psi + \phi$, equations (2.7) combine to give

$$\dot{r} = \frac{f_b}{c_t} \cos(\eta - \phi) \qquad \text{and} \qquad \dot{\eta} = -\frac{f_b}{c_t r} \sin(\eta - \phi) - \frac{k_b r^2}{2c_r(r^2 + \epsilon)} \sin(2\eta). \tag{2.8}$$

A solution with (r, η) constant has $\eta - \phi = \pm \pi/2$, so that

$$0 = -\frac{f_b}{c_t r} + \frac{k_b r^2}{2c_r(r^2 + \epsilon)} \sin(2\phi), \quad \text{or} \quad 0 = c_t k_b \sin(2\phi) r^3 - 2c_r f_b r^2 - 2c_r f_b \epsilon.$$

The discriminant² of this cubic equation is negative since the linear coefficient vanishes and the quadratic and constant coefficients have the same sign. It follows that there are two complex conjugate roots and one real root with expansion

$$r = \frac{c_r}{c_t} \frac{2f_b}{k_b \sin(2\phi)} + \frac{c_t}{c_r} \frac{k_b \sin(2\phi)}{2f_b} \epsilon - 2\left(\frac{c_t}{c_r} \frac{k_b \sin(2\phi)}{2f_b}\right)^3 \epsilon^2 + O(\epsilon^3).$$

2.5.1. Stability. Equation (2.8) has Jacobian matrix

$$F = \begin{bmatrix} 0 & -(f_b/c_t)\sin(\eta - \phi) \\ (f_b/c_tr^2)\sin(\eta - \phi) - \frac{k_b r \epsilon \sin(2\eta)}{c_r(r^2 + \epsilon)^2} & -(f_b/c_t r)\cos(\eta - \phi) - (k_b r^2/c_r(r^2 + \epsilon))\cos(2\eta) \end{bmatrix}.$$

²Recall that the discriminant of the cubic ar^3+br^2+cr+d is $\Delta=18abcd-4b^3d+b^2c^2-4ac^3-27a^2d^2$, which reduces to $\Delta=-4b^3d-27a^2d^2$ when c=0.

The Jacobian at the stationary point becomes

$$F(r,\phi) = \begin{bmatrix} 0 & (f_b/c_t) \\ -\frac{1}{4}(a - \frac{c_t}{f_b}a^2\epsilon + O(\epsilon^2)) & (k_b/c_r)\cos(2\phi)(1 - \frac{1}{4}\frac{c_t}{f_b}a\epsilon) + O(\epsilon^2) \end{bmatrix}$$

where $a \equiv (c_t \sin(2\phi)^2 k_b^2)/(c_r^2 f_b)$. When $\phi = \pi/4$ this becomes

$$F(r, \pi/4) = \begin{bmatrix} 0 & (f_b/c_t) \\ -\frac{1}{4}(a - \frac{c_t}{f_b}a^2\epsilon + O(\epsilon^2)) & 0 \end{bmatrix},$$

which has purely imaginary eigenvalues, so the solutions with constant radii are "marginally" stable.

3. Hydrodynamic interaction. Letting $\mathbf{y}(t) \in \mathbb{R}^2$ denote the position of a bacterium with orientation $\mathbf{m}(t) \in S^1$ and $\mathbf{n}_s(x)$ denote the spiral pattern on the glass plates, we postulate energy and dissipation functions of the liquid crystal medium and bacterium between two glass plates of the form³

$$W(\mathbf{n}, \nabla \mathbf{n}, \mathbf{y}, \mathbf{m}) = \int_{\Omega} W_{OF}(\mathbf{n}(x), \nabla \mathbf{n}(x)) + (\kappa_3/2)|\mathbf{n}(x) - \mathbf{n}_s(x)|^2 dx + W_b(\mathbf{m}, \mathbf{n}(\mathbf{y})),$$
(3.1)

$$\mathcal{R}(\mathbf{v}, \nabla \mathbf{v}, \dot{\mathbf{n}}, \dot{\mathbf{y}}, \dot{\mathbf{m}}; \mathbf{n}, \mathbf{m}) = \int_{\Omega} \mathcal{R}_{EL}(\nabla \mathbf{v}(x), \mathbf{n}(x), \dot{\mathbf{n}}(x)) + (c_3/2)|\mathbf{v}(x)|^2 dx + (c_t/2)|\dot{\mathbf{y}} - \mathbf{v}(\mathbf{y})|^2 + (c_r/2)|\dot{\mathbf{m}} - W(\mathbf{v}(\mathbf{y})\mathbf{m})|^2.$$

In these expressions $W_{OF}(\mathbf{n}, \nabla \mathbf{n})$ and $\mathcal{R}_{EL}(\nabla \mathbf{v}, \mathbf{n}, \dot{\mathbf{n}})$ are the Oseen–Frank elastic energy and the Ericksen–Leslie dissipation functions of the nematic [6, 7, 12, 14, 19];

$$\mathcal{W}_{OF}(\mathbf{n}, \nabla \mathbf{n}) = \frac{1}{2} \left(k_1 \operatorname{div}(\mathbf{n})^2 + k_2 (\mathbf{n}.\operatorname{curl}(\mathbf{n}) + q)^2 + k_3 |\mathbf{n} \times \operatorname{curl}(\mathbf{n})|^2 \right) + \frac{1}{2} (k_2 - k_4) \left(|\nabla \mathbf{n}|^2 - \operatorname{div}(\mathbf{n})^2 - |\operatorname{curl}(\mathbf{n})|^2 \right),$$

and writing $\dot{\mathbf{n}} = \dot{\mathbf{n}} - W(\mathbf{v})\mathbf{n}$

$$\mathcal{R}_{EL}(\mathbf{n}, \dot{\mathbf{n}}, \nabla \mathbf{v}) = \frac{\gamma_1}{2} |\mathring{\mathbf{n}}|^2 + \gamma_2 \mathring{\mathbf{n}}^\top D(\mathbf{v}) \mathbf{n} + \frac{\gamma_3}{2} (D(\mathbf{v}) \mathbf{n})^2 + \frac{\gamma_4}{2} (\mathbf{n}^\top D(\mathbf{v}) \mathbf{n})^2 + \frac{\gamma_5}{2} |D(\mathbf{v})|^2.$$

The terms with coefficients κ_3 and c_3 model the influence of boundary conditions in the third dimension. The elastic constant κ_3 is a measure of the "anchoring strength", and c_3 quantifies the dissipation due to shear in the third dimension due to the fluid sticking to the plates.

³For clarity of exposition \mathcal{W} and \mathcal{R} are written with a single bacterium with position and orientation (\mathbf{y}, \mathbf{m}) . If multiple bacteria are present then \mathcal{W} and \mathcal{R} contain the sum of their elastic energies and rates of dissipation.

Inactive Bacteria: If inactive bacteria are acted upon by an external body force, \mathbf{f}_b , and moment, \mathbf{g}_b , the dynamics would be determined by Hamilton's principle:

$$\delta \int_{t_1}^{t_2} \left(\mathcal{W} - (\rho/2) |\mathbf{v}|^2 \right) + \int_{t_1}^{t_2} \left(\frac{\partial \mathcal{R}}{\partial \dot{\mathbf{y}}} . \delta \mathbf{y} + \frac{\partial \mathcal{R}}{\partial \dot{\mathbf{m}}} . \delta \mathbf{m} + \frac{\partial \mathcal{R}}{\partial \mathbf{v}} . \delta \mathbf{x} + \frac{\partial \mathcal{R}}{\partial \nabla \mathbf{v}} : \nabla \delta \mathbf{x} + \frac{\partial \mathcal{R}}{\partial \dot{\mathbf{n}}} . \delta \mathbf{n} \right)$$

$$= \int_{t_1}^{t_2} \left(\mathbf{f}_b . \delta \mathbf{y} + \mathbf{g}_b . \delta \mathbf{m} + \mathbf{f} . \delta \mathbf{x} + \mathbf{g} . \delta \mathbf{n} \right) .$$

As in Section 2, variations of \mathbf{y} and \mathbf{m} give the equations (2.2) for of motion for the bacteria. Variations of x and \mathbf{n} give the linear and angular momentum balances for the liquid crystal which we assume to be incompressible,

$$\rho \dot{\mathbf{v}} + c_3 \mathbf{v} - \operatorname{div} \left[-pI + \frac{\partial \mathcal{R}_{EL}}{\partial \nabla \mathbf{v}} - (\nabla \mathbf{n})^{\top} \frac{\partial \mathcal{W}_{OF}}{\partial \nabla \mathbf{n}} \right] + \kappa_3 (\nabla \mathbf{n})^{\top} (\mathbf{n} - \mathbf{n}_s)$$

$$-\mathbf{f}_b \delta_{\mathbf{y}} - c_r W^* \left(\dot{\mathbf{m}} - W(\mathbf{v}(\mathbf{y})) \mathbf{m} \right) \otimes \mathbf{m} \right) = \mathbf{f},$$

$$\frac{\partial \mathcal{R}_{EL}}{\partial \dot{\mathbf{n}}} + \frac{\partial W_{OF}}{\partial \mathbf{n}} - \operatorname{div} \left[\frac{\partial \mathcal{W}}{\partial \nabla \mathbf{n}} \right] + \kappa_3 (\mathbf{n} - \mathbf{n}_s) + \frac{\partial \mathcal{W}_b}{\partial \mathbf{n}} \delta_{\mathbf{y}} + \lambda \mathbf{n} = \mathbf{g}.$$
(3.2)

Here $\delta_{\mathbf{y}}$ and $W^*(.)$ are distributions which act on scalar and vector valued test functions respectively as $\delta_{\mathbf{y}}(\phi) = \phi(t, \mathbf{y}(t))$ and

$$W^*(A)(\phi) = A : (1/2) \left(\nabla \phi(t, \mathbf{y}(t)) - \nabla \phi(t, \mathbf{y}(t))^\top \right) \equiv A : W(\phi(\mathbf{y})).$$

Active Bacteria: When the motion of the bacteria is due to their swimming action, and the bacteria have negligible inertia, the active force generated by the flagellum and the drag on the body of the bacteria are equal in magnitude and opposite in direction as illustrated in Figure 3.1. However, their action on the fluid is displaced by a distance, ℓ , comparable to the length of the bacteria which is small. In this situation the active forces on the fluid can be approximated by a dipole [3]; specifically, if ϕ is a vector valued test function, then (see Figure 3.1)

$$\mathbf{f}_b.\boldsymbol{\phi}\left(\mathbf{y}+(\ell/2)\mathbf{m}\right)-\mathbf{f}_b.\boldsymbol{\phi}\left(\mathbf{y}-(\ell/2)\mathbf{m}\right)\simeq \ell(\mathbf{f}_b\otimes\mathbf{m}):\nabla\boldsymbol{\phi}(\mathbf{y})\equiv \operatorname{div}^*(\ell\mathbf{f}_b\otimes\mathbf{m})(\boldsymbol{\phi}).$$

The linear momentum equation for the active system is then obtained by substituting this distribution in place of the inactive force $\mathbf{f}_b \delta_{\mathbf{y}}$ in (3.2). Since $\mathbf{f}_b = f_b \mathbf{m}$, the dipole $\ell \mathbf{f}_b \otimes \mathbf{m} = (\ell f_b) \mathbf{m} \otimes \mathbf{m}$ is symmetric so does not couple to the angular momentum equation.

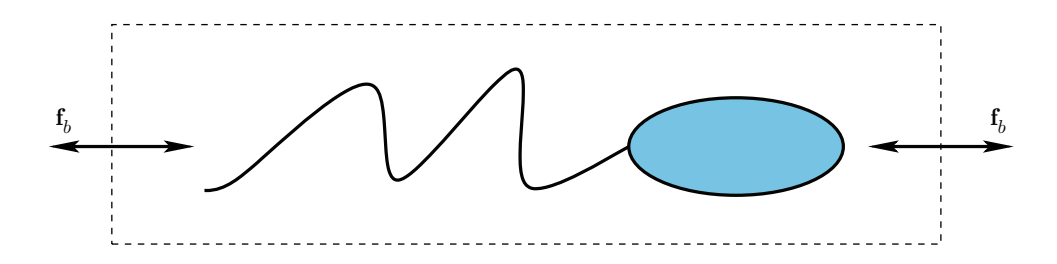


Fig. 3.1. Forces on the tail (active), head (drag), and fluid (dipole).

Collecting the above gives the following set of equations for the coupled system,

$$c_{t}(\dot{\mathbf{y}} - \mathbf{v}) + (\nabla \mathbf{n})^{\top} \frac{\partial \mathcal{W}_{b}}{\partial \mathbf{n}} = f_{b} \mathbf{m},$$

$$c_{r}(\dot{\mathbf{m}} - W(\mathbf{v}(\mathbf{y}))\mathbf{m}) + \frac{\partial \mathcal{W}_{b}}{\partial \mathbf{m}} + \lambda_{b} \mathbf{m} = 0,$$

$$\rho \dot{\mathbf{v}} + c_{3} \mathbf{v} - \operatorname{div} \left[-pI + \frac{\partial \mathcal{R}_{EL}}{\partial \nabla \mathbf{v}} - (\nabla \mathbf{n})^{\top} \frac{\partial \mathcal{W}_{OF}}{\partial \nabla \mathbf{n}} \right] + \kappa_{3} (\nabla \mathbf{n})^{\top} (\mathbf{n} - \mathbf{n}_{s})$$

$$- \operatorname{div}^{*} (f_{b} \ell \mathbf{m} \otimes \mathbf{m}) - c_{r} W^{*} \left(\dot{\mathbf{m}} - W(\mathbf{v}(\mathbf{y})) \mathbf{m} \right) \otimes \mathbf{m} \right) = \mathbf{f},$$

$$\frac{\partial \mathcal{R}_{EL}}{\partial \dot{\mathbf{n}}} + \frac{\partial \mathcal{W}_{OF}}{\partial \mathbf{n}} - \operatorname{div} \left[\frac{\partial \mathcal{W}}{\partial \nabla \mathbf{n}} \right] + \kappa_{3} (\mathbf{n} - \mathbf{n}_{s}) + \frac{\partial \mathcal{W}_{b}}{\partial \mathbf{n}} \delta_{\mathbf{y}} + \lambda \mathbf{n} = \mathbf{g}.$$
(3.3)

The variables (λ_b, p, λ) are Lagrange multipliers dual to the constraints $|\mathbf{m}| = 1$, $\operatorname{div}(\mathbf{v}) = 0$ and $|\mathbf{n}| = 1$ respectively.

3.1. Weak statement & energy estimate. The (Ericksen) identity [19]

$$\operatorname{div}\left[\left(\nabla\mathbf{n}\right)^{\top}\frac{\partial\mathcal{W}_{OF}}{\partial\nabla\mathbf{n}}\right] = \nabla\mathcal{W}_{OF} - \left(\nabla\mathbf{n}\right)^{\top}\left(\frac{\partial\mathcal{W}_{OF}}{\partial\mathbf{n}} - \frac{\partial\mathcal{W}_{OF}}{\partial\nabla\mathbf{n}}\right),$$

is used to formulate a weak statement of the system for which Galerkin approximations inherit the natural energy estimates. Using this identity, and writing $\mathbf{\mathring{m}} = \dot{\mathbf{m}} - W(\mathbf{v}(\mathbf{y}))\mathbf{m}$ and $\hat{p} = p + \mathcal{W}_{OF}$, we have

$$\int_{\Omega} \left\{ \left(\rho \dot{\mathbf{v}} + c_3 \mathbf{v}, \bar{\mathbf{v}} \right) - \left(\hat{p}, \operatorname{div}(\bar{\mathbf{v}}) \right) + \left(\frac{\partial \mathcal{R}_{EL}}{\partial \nabla \mathbf{v}}, \nabla \bar{\mathbf{v}} \right) + \left(\frac{\partial \mathcal{R}_{EL}}{\partial \dot{\mathbf{n}}}, (\nabla \mathbf{n}) \bar{\mathbf{v}} \right) \right\} = \int_{\Omega} \left(\mathbf{f} + (\nabla \mathbf{n})^{\top} \mathbf{g}, \bar{\mathbf{v}} \right) \\
+ f_b \ell \left(\mathbf{m} \otimes \mathbf{m}, \nabla \bar{\mathbf{v}}(\mathbf{y}) \right) - \left(\frac{\partial \mathcal{W}_b}{\partial \mathbf{n}}, \nabla \mathbf{n}(\mathbf{y}) \bar{\mathbf{v}}(\mathbf{y}) \right) + c_r \left(\mathring{\mathbf{m}} \otimes \mathbf{m}, W(\bar{\mathbf{v}}(\mathbf{y})) \right), \quad (3.4)$$

$$\int_{\Omega} \left\{ \left(\frac{\partial \mathcal{R}_{EL}}{\partial \dot{\mathbf{n}}} + \frac{\partial W_{OF}}{\partial \mathbf{n}} + \kappa_3 (\mathbf{n} - \mathbf{n}_s) + \lambda \mathbf{n}, \bar{\mathbf{n}} \right) + \left(\frac{\partial \mathcal{W}_{OF}}{\partial \nabla \mathbf{n}}, \nabla \bar{\mathbf{n}} \right) \right\} = \int_{\Omega} (\mathbf{g}, \bar{\mathbf{n}}) - \left(\frac{\partial \mathcal{W}_b}{\partial \mathbf{n}}, \bar{\mathbf{n}}(\mathbf{y}) \right).$$

Here $\bar{\mathbf{v}}$ and $\bar{\mathbf{n}}$ are test functions and homogeneous boundary conditions have been assumed. The energy estimate follows upon multiplying the equations for \mathbf{y} and \mathbf{m} by $\dot{\mathbf{y}} - \mathbf{v}$ and $\dot{\mathbf{m}}$ respectively, and selecting the test functions in this weak statement $(\bar{\mathbf{v}}, \bar{\mathbf{n}}) = (\mathbf{v}, \mathbf{n}_t)$ to get

$$\frac{d}{dt} \left(\mathcal{W} + \int_{\Omega} (\rho/2) |\mathbf{v}|^{2} \right) + \int_{\Omega} \left(\frac{\partial \mathcal{R}_{EL}}{\partial \dot{\mathbf{n}}} . \dot{\mathbf{n}} + \frac{\partial \mathcal{R}_{EL}}{\partial \nabla \mathbf{v}} : (\nabla \mathbf{v}) \right) + c_{3} |\mathbf{v}|^{2} + c_{t} |\dot{\mathbf{y}} - \mathbf{v}(\mathbf{y})|^{2} + c_{r} |\dot{\mathbf{m}}|^{2}$$

$$= \int_{\Omega} \left(\mathbf{f} . \mathbf{v} + \mathbf{g} . \dot{\mathbf{n}} \right) + f_{b} \mathbf{m} . (\dot{\mathbf{y}} - \mathbf{v}(\mathbf{y})) + f_{b} \ell(\mathbf{m} \otimes \mathbf{m}) : (\nabla \mathbf{v}(\mathbf{y})).$$

- 3.2. Scaling. To render equations (3.3) dimensionless, we scale them using typical values of mass, length, and time present in the experiments reported in [11, 26, 27].
 - $M = 10^{-9} kg$, the mass of fluid in the experiment.
 - $L = 10^{-3} m$, the size of the cell.
 - T = 10s, experimental data was recorded for approximately 10 minutes.

Table 3.1 lists the physical parameters and scaled values of the coefficients appearing in equations (3.3).

Coefficient	Unit	Scale Factor	Value	Scaled Value
Mass	M	10 ⁹	$1\mu g$	1
Length	L	10^{3}	$1\ mm$	1
Time	T	10^{-1}	10 s	1
Bacteria Dynamics				
c_t Transnational Viscosity	$\frac{M}{T}$	10^{10}	2×10^{-9}	20
c_r Rotational Viscosity	$\frac{ML^2}{T}$	10^{16}	2.5×10^{-17}	0.25
f_b Active Force	$\frac{\dot{M}L}{T^2}$	10^{14}	2×10^{-14}	2
k_b Elastic Constant	$\frac{\frac{ML^2}{T}}{\frac{ML}{T^2}}$ $\frac{\frac{ML}{T^2}}{\frac{ML^2}{T^2}}$	10^{17}	1×10^{-18}	0.1
Nematic Hydrodynamics				
ρ Density	$\frac{M}{I3}$	1	1000	1000
k_i Elastic Coefficients	$\frac{ML}{T^2}$	10^{14}	$[7.5, 0.6, 21, 0] \times 10^{-15}$	[0.75, 0.06, 2.1, 0]
γ_i Viscous Coefficients	$\frac{M}{LT}$	10^{7}	$[0.15, 0.35, 1.75, 0.1, 1] \times 10^{-7}$	[0.15, 0.35, 1.75, 0.1, 1]
κ_3 Anchoring Strength	$ \frac{\frac{M}{L^3}}{\frac{M}{L}} $ $ \frac{\frac{M}{L}}{T^2} $ $ \frac{M}{LT} $ $ \frac{M}{LT^2} $ $ \frac{M}{LT^2} $	10^{8}	2×10^{-7}	20
c ₃ Shear Viscosity	$\frac{L_{M}^{I}}{2}$	10	5	50

Table 3.1. Scale factors for non-dimensionalization.

4. Numerical approximation. The ODE's for the bacteria positions and orientations were solved using the classical fourth order Runge-Kutta algorithm with the equations (2.2) formulated as

$$c_t(\dot{\mathbf{y}} - \mathbf{v}) + (\nabla \mathbf{n})^{\top} \frac{\partial \hat{\mathcal{W}}_b}{\partial \mathbf{n}} = f_b \mathbf{m}, \quad \text{and} \quad c_r(\dot{\psi} - \omega(\mathbf{y})/2) + \frac{\partial \hat{\mathcal{W}}_b}{\partial \psi} = 0,$$

where $\mathbf{m} = (\cos(\psi), \sin(\psi))$, $\omega = \text{curl}(\mathbf{v})$ is the vorticity, and $\hat{\mathcal{W}}(\psi, \mathbf{n}) = \mathcal{W}(\mathbf{m}(\psi), \mathbf{n})$; specifically,

$$\omega = \frac{\partial v_2}{\partial x_1} - \frac{\partial v_1}{\partial x_2}, \quad \text{and} \quad \frac{\partial \hat{\mathcal{W}}_b}{\partial \psi}(\psi, \mathbf{n}) = \frac{\partial \mathcal{W}_b}{\partial \mathbf{m}}(\mathbf{m}, \mathbf{n}). \begin{pmatrix} -\sin(\psi) \\ \cos(\psi) \end{pmatrix}.$$

The equations for the nematic were approximated using the numerical scheme in [23]. This is a Galerkin approximation of equations (3.4) with discontinuous Galerkin time stepping for the linear momentum equation and continuous Galerkin time stepping for the angular momentum equation. The constraint $|\mathbf{n}| = 1$ is approximated by including a penalty term $(1/\epsilon)(|\mathbf{n}|^2 - 1)^2$ into the energy \mathcal{W} . This scheme was coded using the Firedrake finite element package [17]. The distributions on the right hand side of equations (3.4) were approximated using a Gaussian mollifier of the form $\delta_{\mathbf{y}(t)}(t,x) \simeq \exp(-|x-\mathbf{y}(t)|^2/\epsilon)/(\epsilon\pi)$; for example

$$(\mathbf{m}(t) \otimes \mathbf{m}(t), \nabla \bar{\mathbf{v}}(t, \mathbf{y}(t))) \simeq \int_{\Omega} (\mathbf{m}(t) \otimes \mathbf{m}(t), \nabla \bar{\mathbf{v}}(t, x)) \exp(-|x - \mathbf{y}(t)|^2 / \epsilon) / (\epsilon \pi) dx.$$

When $\mathbf{y}(t)$ and $\mathbf{m}(t)$ are specified, Firedrake can evaluate the right hand side of this expression but not the left. Anisotropic Gaussian's with $(x - \mathbf{y})^{\top} M(x - \mathbf{y})$ in place of $|x - \mathbf{y}|^2$ were considered in [8] with $M = g_{\parallel}(\mathbf{m} \otimes \mathbf{m}) + g_{\perp}(I - \mathbf{m} \otimes \mathbf{m})$; however, numerical solutions were essentially identical for the isotropic and anisotropic Gaussian's.

Being a finite element package, Firedrake can only approximate solutions of the PDE's for \mathbf{v} and \mathbf{n} so it is necessary to utilize a partitioned time stepping scheme to solve the coupled system. Writing $X = (\mathbf{y}, \mathbf{m})$ and $Y = (\mathbf{v}, \mathbf{n})$, the time stepping in the following lemma was utilized.

LEMMA 4.1. Let $[t^k, t^k + \tau] \subset \mathbb{R}$ with $\tau > 0$,

$$F: [t^k, t^k + \tau] \times \mathbb{R}^m \times \mathbb{R}^n \to \mathbb{R}^m$$
 and $G: [t^k, t^k + \tau] \times \mathbb{R}^m \times \mathbb{R}^n \to \mathbb{R}^n$,

and $(X,Y):[t^k,t^k+\tau]\to\mathbb{R}^m\times\mathbb{R}^n$ satisfy

$$\dot{X} = F(., X, Y), \quad \dot{Y} = G(., X, Y), \quad \text{with} \quad (X, Y)(t^k) = (X^k, Y^k) \in \mathbb{R}^m \times \mathbb{R}^n.$$

Let

$$\dot{X}_1 = F(., X_1, Y^k), \quad \dot{Y}_1 = G(., X_1, Y_1), \quad \text{with} \quad (X_1, Y_1)(t^k) = (X^k, Y^k)$$

 $\dot{X}_2 = F(., X_2, Y_1), \quad \dot{Y}_2 = G(., X_2, Y_2), \quad \text{with} \quad (X_2, Y_2)(t^k) = (X^k, Y^k).$

Then the scheme $(X^{k+1}, Y^{k+1}) = (X_2(t+\tau), Y_2(t+\tau))$ is third order with local truncation error

$$|X^{k+1} - X(t+\tau)| \le (1/4!)L_F^2 L_G L_Y e^{\tau(L_G + 2L_F)} \tau^4,$$

$$|Y^{k+1} - Y(t+\tau)| \le (1/5!)L_F^2 L_G^2 L_Y e^{2\tau(L_F + L_G)} \tau^5,$$

where L_F , L_G , L_X , and L_Y denote the Lipschitz constants of the indicated functions.

Identifying $\dot{X} = F(., X, Y)$ as the system of ODE's for the bacteria and $\dot{Y} = G(., X, Y)$ as the Galerkin approximation of the PDE's modeling the nematic, this scheme requires two decoupled Runge Kutta solves and finite element solutions per time step.

- 5. Numerical results. The domain and parameters were selected to model the experimental configuration in [11, 26, 27], and non-dimensionalized as in Section 3.2.
 - Domain: $\Omega = [-1, 1]^2$.
 - Constraint: The constraint $|\mathbf{n}| = 1$ was approximated by adding $(1/\epsilon)(|\mathbf{n}|^2 1)^2$ to the bulk term of the elastic energy in equation (3.1). The penalty parameter was set to be $\epsilon = 0.01$.
 - Spiral Pattern: $\mathbf{n}_s(x)$ is given in equation (2.3). Unless noted otherwise, the parameter characterizing the size of the core of the singularity was set to be $\epsilon = 0.1$
 - Boundary Data: $\mathbf{v}|_{\partial\Omega} = 0$ and $\mathbf{n}(t,x)|_{\partial\Omega} = \mathbf{n}_s(x)$.
 - Initial Data:
 - Velocity: $\mathbf{v}(0,x) = \mathbf{0}$
 - Director: For the hydrodynamic simulations $\mathbf{n}(0, x)$ was set to be a (numerically computed) minimizer of the elastic energy given by the bulk term in equation (3.1) augmented with the penalty term to approximate the constraint $|\mathbf{n}| = 1$.
 - Note that the spiral pattern $\mathbf{n}_s(x)$ is not a minimizer of the Oseen Frank energy \mathcal{W}_{OF} . Selecting the initial value to be a minimizer of (3.1) rather than $\mathbf{n}_s(x)$ eliminates an initial transient.

- Bacteria Orientation: Unless otherwise noted, the bacteria are initially (inwardly) aligned with the spiral, $\mathbf{m}(0) = -\mathbf{n}_s(\mathbf{y}(0))$; specifically, $\psi(0) = \pi \phi \theta(0)$.
 - Solutions of the ODE's (2.4) with initial angles outwardly aligned with the spiral, $\psi(0) \in (\phi + \theta(0) \pi/2, \phi + \theta(0) + \pi/2)$, directly exit the domain.
- Mollifier: The parameter in the Gaussian mollifier of $\delta_{\mathbf{y}}$ was $\epsilon = 0.24$.
- Physical Parameters: The elastic and viscous parameters are listed in Table 3.1.
- 5.1. ODE system. The position and orientation of active bacteria were simulated by solving the ODE system with initial values $\mathbf{y}(0) = (0.67, 0)$ and $\psi(0) = -\pi/2$, so that $\mathbf{m}(0)$ is tangential to the circular solutions. The radii $r(\phi)$ of the solutions with circular orbits are

$$r(\pi/6) = 0.682,$$
 $r(\pi/4) = 0.613,$ $r(\pi/3) = 0.672.$

Figure 5.1 plots numerical solutions for Equation 2.2 with spiral angles $\phi = \pi/6$, $\pi/4$ and $\pi/3$ to illustrate the unstable, marginally stale, and stable cases respectively. With $\phi = \pi/6$ and initial position and orientation close to a point on the circular solution of Equation (2.2), the bacteria makes one orbit of the circular equilibrium and then enters the invariant region in which the radius increases monotonically. The middle panels illustrate the solution with spiral angle $\phi = \pi/4$ which is the configuration considered in Example 2.4. The circular solution is marginally stable when $\epsilon = 0$, and is slightly unstable for for $\epsilon = 0.1$. The latter situation is illustrated in Figure 5.1 where the bacteria traverse a spiral with slowly increasing radius. When the spiral angle is $\pi/3$, the bacteria travel in a circular motion with a fixed radius and the trajectory converges to the stable equilibrium in the phase plane.

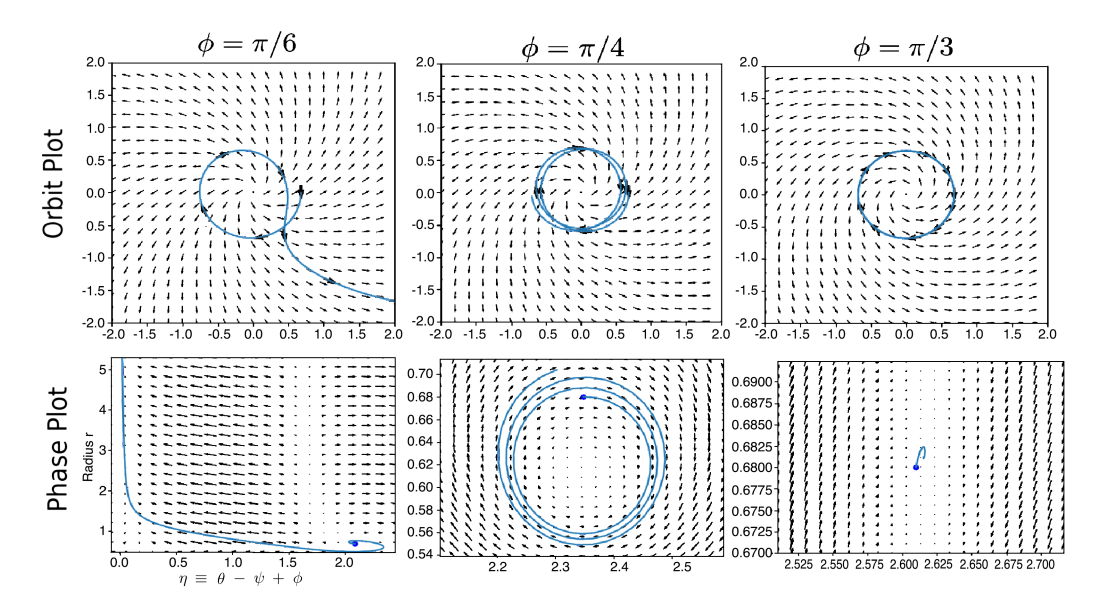


Fig. 5.1. Orbits and phase plots for single bacteria with spiral angles $\pi/6$, $\pi/4$, and $\pi/3$.

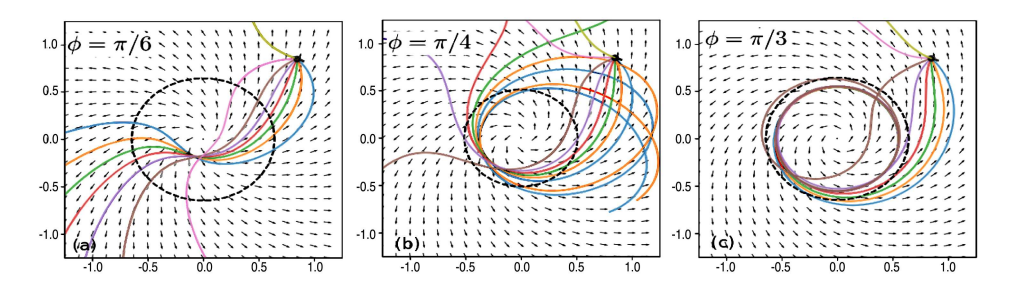


Fig. 5.2. Multiple initial angles for a single bacteria: Trajectories with spiral angle $\pi/6$, $\pi/4$, and $\pi/3$.

To illustrate how the trajectories depend up the initial orientations Figure 5.2 plots multiple solutions with multiple initial orientations emanating from a fixed point for three spiral angles.

- $\phi = \pi/6$: All trajectories eventually exit the domain following the spiral director pattern.
- $\phi = \pi/4$: The bacteria initially move towards the equilibrium circle before spiraling out of the domain with the number circular orbits traversed depending upon their initial angle. Experimental observation of bacteria motion with this spiral angle exhibit a similar range of outcomes.
- $\phi = \pi/3$: The circular solution is stable and attracts most of the solutions.

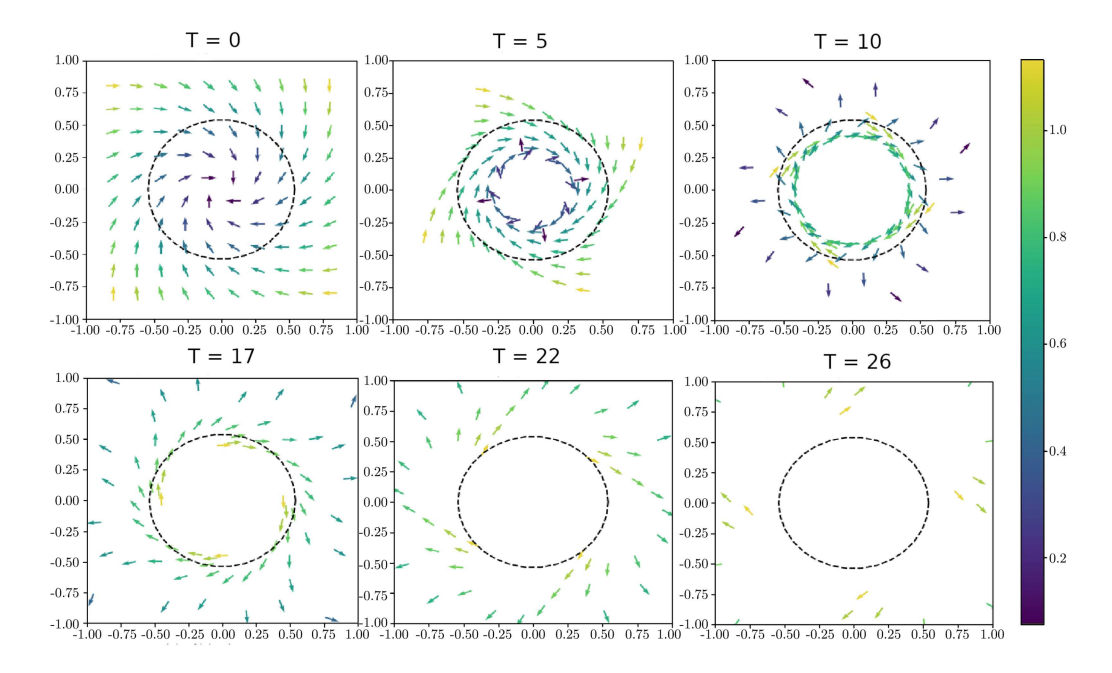


Fig. 5.3. Time slices of solutions of the ODE's with spiral angle $\pi/4$ and bacteria initially on a 10×10 grid.

To simulate the patterns that may be observed when bacteria are uniformly distributed, solutions of the ODE with bacteria initially on a 10×10 grid are shown in Figure 5.3. The bacteria were initially aligned inwardly with the spiral having angle $\phi = \pi/4$, and colored by the radius of their initial positions. The bacteria exhibit transient behavior; traveling in a circular motion, they first concentrate on a circle with radius less than the stationary value. The radius of the circle where they concentrate slowly increases, and after reaching the stationary radius spiral outwards to exit the domain with bacteria initially at smaller radii exiting first.

5.2. Partial hydrodynamics ($\mathbf{v} = 0$). The gap between the glass plates in the experiments in [11] was small, and since the fluid sticks to the plates the the velocity was observed to be very small, $\mathbf{v} \simeq 0$. This section considers the solution of equations (3.3) with $\mathbf{v} \equiv 0$, in which case the hydrodynamic interaction only involves the elastic interaction with the nematic. With this ansatz equations (3.3) reduce to a system of vector valued ODE's for the bacteria positions and orientations coupled to the angular momentum equation for the nematic. Solutions of these equations were approximated using the classical fourth order Runge Kutta scheme for the ODE's and finite elements for the angular momentum equation with quadratic bilinear elements on a 32×32 grid with time step $\Delta t = 0.01$. The qualitative behavior of the solutions reported here did not change under further refinement of the mesh or time step.

The experimental observations in [11] indicated that in low concentrations the bacteria tended to simply follow the spiral pattern, while at higher concentration they were more likely to swim in circular orbits. In the current context we illustrate similar trends when "concentration" is identified with with hydrodynamic interaction which depends primarily upon the active force f_b and elastic constant k_b . Another possible consequence of increased bacteria concentration is that, being rod like, they will tend to align with each other. In this situation their initial orientation may not be aligned with the spiral pattern, and this can also result in more bacteria swimming in circular trajectories.

Figure 5.4–5.6 illustrate these trends. Figure 5.4 shows the numerical solution of the configuration shown in Figure 5.3 when the hydrodynamic interaction is included. The hydrodynamics results in a dramatic difference to the long time behavior of the system. Absent the hydrodynamics, all of the bacteria eventually exit the domain; however, Figure 5.4 clearly shows that approximately half of the bacteria remain and swim in circular orbits with a time periodic radius [11].

Figure 5.5 illustrates the role of both hydrodynamics and influence of initial bacteria orientation on the solutions. The spiral angle was set to $\phi = \pi/6$ so that circular solutions of the ODE's (2.4) are unstable (as illustrated in Figure 5.2). The left two panels of Figure 5.5 show solutions at a fixed time for the ODE's and the coupled system with the bacteria initially aligned with the spiral $\psi(0) = \pi + \phi + \theta(0)$, and the right hand panel shows the solution of the coupled system when $\psi(0) = 9\pi/8 + \phi + \theta(0)$. It is clear that both the hydrodynamics and initial orientation significantly influence the collective dynamics of the bacteria.

To further illustrate the effect of initial bacteria orientation, solutions with four closely spaced bacteria and spiral angle $\phi=\pi/4$ are illustrated in Figure 5.6. Solutions of the ODE's with bacteria initially aligned with the spiral all exit the domain; however, when the initial orientation of the top two bacteria is perturbed those two bacteria remain in the domain and tend to circular orbits. The hydrodynamic interaction results in a similar scenario; instead of exiting the domain when initially aligned with the spiral the bacteria tend to a circular orbit.

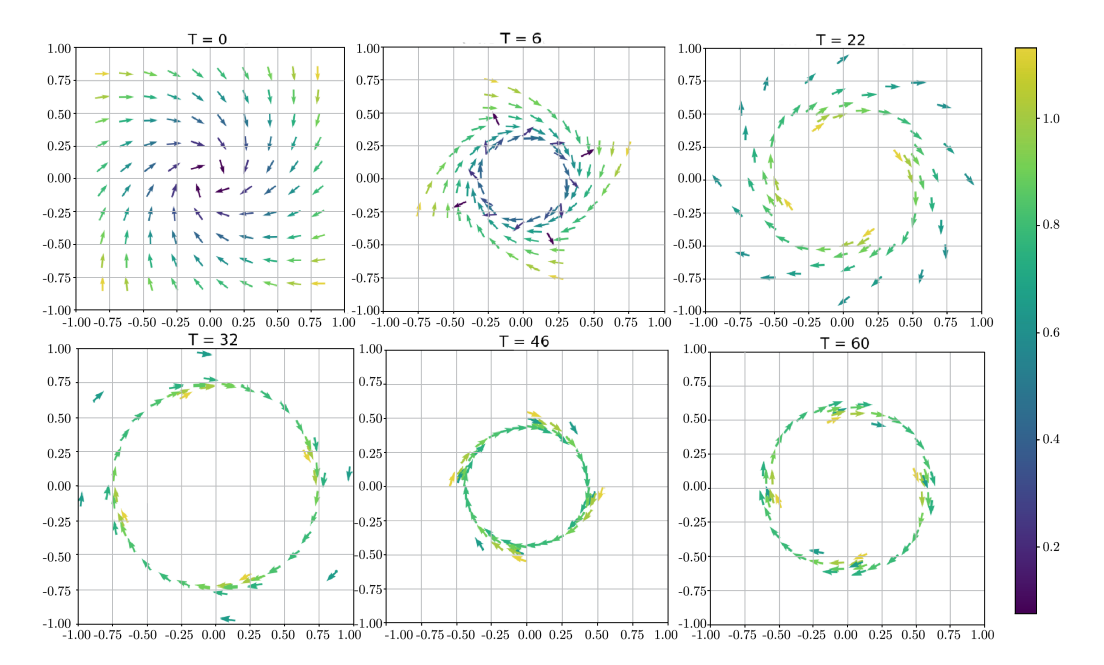


Fig. 5.4. Partial hydrodynamics $\mathbf{v}(t,x) = \mathbf{0}$: spiral angle $\phi = \pi/4$ and bacteria initially on a 10×10 grid.

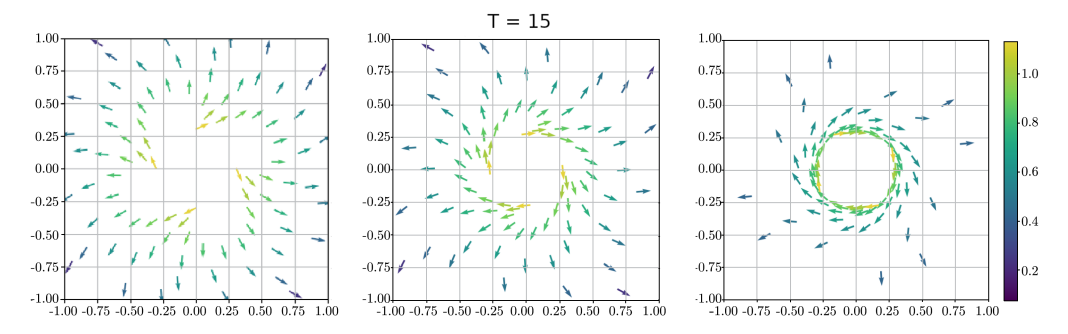


Fig. 5.5. Solutions at time t=15 for ODE's (left), partial hydrodynamics initially aligned (middle), and not aligned (right) with the spiral having angle of $\phi = \pi/6$.

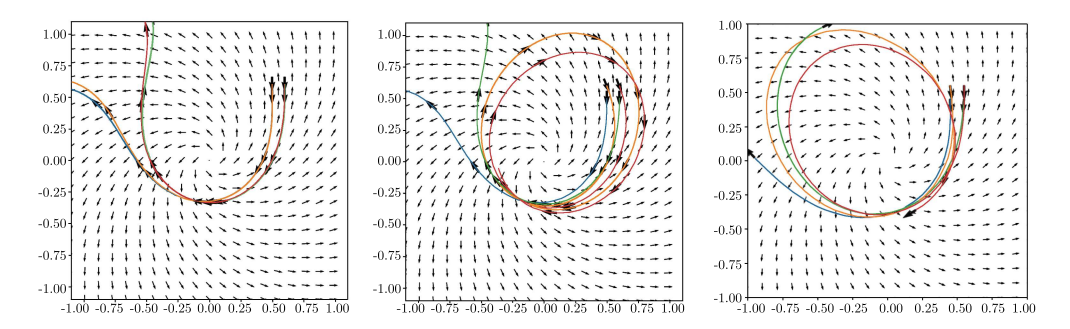


FIG. 5.6. Solutions of the ODE with bacteria initially aligned (left) and perturbed (middle) with the spiral, and solution with partial hydrodynamics (right).

5.3. Full hydrodynamics. This section presents numerical approximations of solutions to the ODE's modeling the bacteria motion with the full set of hydrodynamic equations in equations (3.3). As in the experiments, the velocity of the nematic was small so relaxing the assumption $\mathbf{v} = 0$ made in the previous section resulted in very little change.

Figure 5.7 illustrates the velocity field generated by a single bacterium initially aligned with a spiral with angle $\phi = \pi/4$. This is the configuration illustrated in Figure 5.6 where

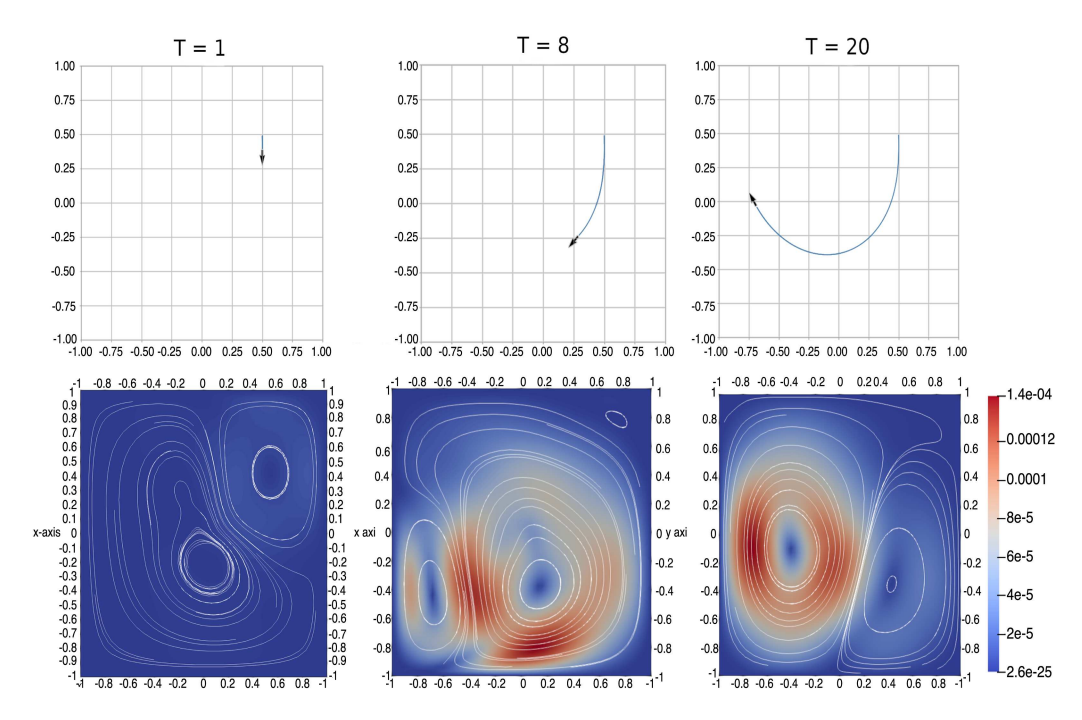


FIG. 5.7. Trajectory and velocity streamlines for a single bacterium initially aligned with the spiral having angle $\phi = \pi/4$.

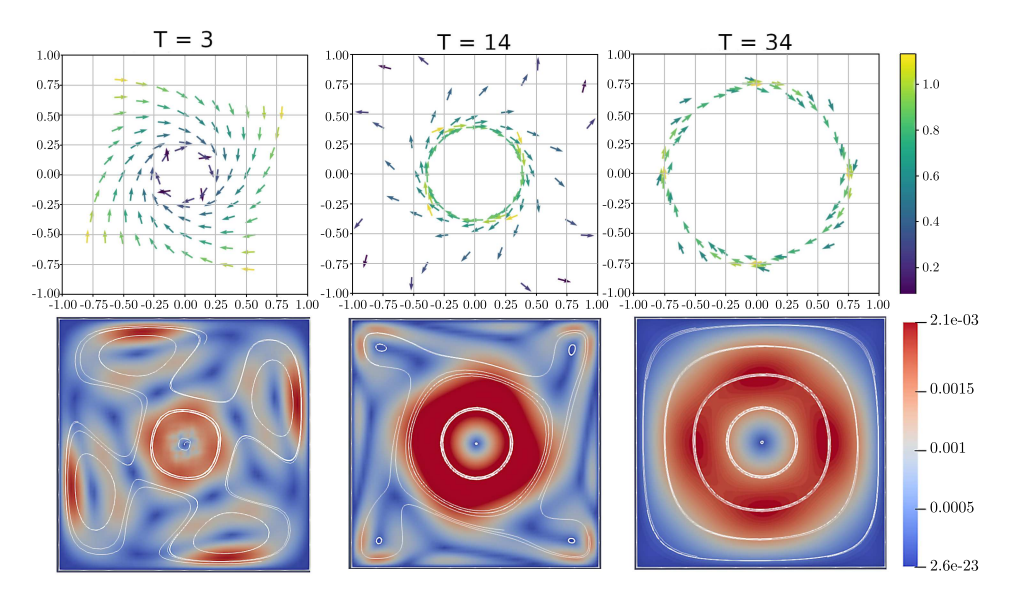


Fig. 5.8. Trajectories and velocity streamlines for 100 bacteria initially aligned with the spiral having angles $\phi = \pi/4$.

the the bacterium eventually exits the domain. Figure 5.8 illustrates the solution for the configuration shown in Figures 5.3 and 5.4. The solution is qualitatively the same as for the partial hydrodynamics considered in the previous section, and the only quantitative change is that of the initial 100 bacteria 68 remained in the domain while only 54 remained in Figure 5.4

References

- [1] F. Alouges, A. DeSimone, and A. Lefebvre, Optimal strokes for low Reynolds number swimmers: an example, J. Nonlinear Sci. 18 (2008), no. 3, 277–302, DOI 10.1007/s00332-007-9013-7. MR2411380
- [2] G. K. Batchelor, An introduction to fluid dynamics, Second paperback edition, Cambridge Mathematical Library, Cambridge University Press, Cambridge, 1999. MR1744638
- [3] X. Chen and J.-G. Liu, Global weak entropy solution to Doi-Saintillan-Shelley model for active and passive rod-like and ellipsoidal particle suspensions, J. Differential Equations 254 (2013), no. 7, 2764–2802, DOI 10.1016/j.jde.2013.01.005. MR3017030
- [4] A. DeSimone, F. Alouges, and A. Lefebvre, Biological fluid dynamics, non-linear partial differential equations, Mathematics of complexity and dynamical systems. Vols. 1–3, Springer, New York, 2012, pp. 26–31, DOI 10.1007/978-1-4614-1806-1_3. MR3220660
- [5] A. DeSimone, F. Alouges, and A. Lefebvre, Biological fluid dynamics, non-linear partial differential equations, Mathematics of complexity and dynamical systems. Vols. 1–3, Springer, New York, 2012, pp. 26–31, DOI 10.1007/978-1-4614-1806-1_3. MR3220660
- [6] J. L. Ericksen, Nilpotent energies in liquid crystal theory, Arch. Rational Mech. Anal. 10 (1962), 189–196, DOI 10.1007/BF00281186. MR169513
- [7] F. C. Frank, On the theory of liquid crystals, Discuss. Faraday Soc., 25 (1958), pp. 19–28.
- [8] M. Genkin, A. Sokolov, O. Lavrentovich, and I. Aranson, Topological defects in a living nematic ensnare swimming bacteria, Physical Review X, 7 (2017).
- [9] M. M. Genkin, A. Sokolov, and I. S. Aranson, Spontaneous topological charging of tactoids in a living nematic, New Journal of Physics, 20 (2018), p. 043027.
- [10] G. B. Jeffery, The motion of ellipsoidal particles immersed in a viscous fluid, Proc. Royal Society London, 102 (1922), pp. 161–179.

- [11] R. Koizumi, T. Turiv, M. M. Genkin, R. J. Lastowski, H. Yu, I. Chaganava, Q.-H. Wei, I. S. Aranson, and O. D. Lavrentovich, Control of microswimmers by spiral nematic vortices: Transition from individual to collective motion and contraction, expansion, and stable circulation of bacterial swirls, Phys. Rev. Research, 2 (2020), p. 033060.
- [12] F. Leslie, Theory of flow phenomenum in liquid crystals, in The Theory of Liquid Crystals, W. Brown, ed., vol. 4, New York, 1979, Academic Press., pp. 1–81.
- [13] M. C. Marchetti, J. F. Joanny, S. Ramaswamy, T. B. Liverpool, J. Prost, M. Rao, and R. A. Simha, Hydrodynamics of soft active matter, Rev. Mod. Phys., 85 (2013), pp. 1143–1189.
- [14] G. Marrucci and F. Greco, Flow behavior of liquid crystalline polymers, in Advances in Chemical Physics, I. Prigogine and S. A. Rice, eds., vol. LXXXVI, John Wiley & Sons, Inc., 1993, pp. 331–404.
- [15] A. Panchenko, D. F. Hinz, and E. Fried, Spatial averaging of a dissipative particle dynamics model for active suspensions, Physics of Fluids, 30 (2018).
- [16] C. Peng, T. Turiv, Y. Guo, Q.-H. Wei, and O. Lavrentovich, Command of active matter by topological defects and patterns, Science 354 (2016), pp. 882–885.
- [17] F. Rathgeber, D. A. Ham, L. Mitchell, M. Lange, F. Luporini, A. T. T. McRae, G.-T. Bercea, G. R. Markall, and P. H. J. Kelly, Firedrake: automating the finite element method by composing abstractions, ACM Trans. Math. Software 43 (2017), no. 3, Art. 24, 27, DOI 10.1145/2998441. MR3615280
- [18] D. Saintillan and M. J. Shelley, Active suspensions and their nonlinear models: Living fluids / Fluides vivants, Comptes Rendus Physique, 14 (2013), pp. 497–517.
- [19] A. M. Sonnet and E. G. Virga, Dissipative ordered fluids, Springer, New York, 2012. Theories for liquid crystals, DOI 10.1007/978-0-387-87815-7. MR2893657
- [20] J. Toner and Y. Tu, Long-range order in a two-dimensional dynamical xy model: How birds fly together, Physical Review Letters, 75 (1995), pp. 4326–4329.
- [21] J. Toner and Y. Tu, Flocks, herds, and schools: a quantitative theory of flocking, Phys. Rev. E (3) 58 (1998), no. 4, 4828–4858, DOI 10.1103/PhysRevE.58.4828. MR1651324
- [22] J. Toner, Y. Tu, and S. Ramaswamy, Hydrodynamics and phases of flocks, Ann. Physics 318 (2005), no. 1, 170–244, DOI 10.1016/j.aop.2005.04.011. MR2148645
- [23] N. J. Walkington, Numerical approximation of nematic liquid crystal flows governed by the Ericksen-Leslie equations, ESAIM Math. Model. Numer. Anal. 45 (2011), no. 3, 523–540, DOI 10.1051/m2an/2010065. MR2804649
- [24] J. Walton, G. McKay, M. Grinfeld, and N. J. Mottram, *Pressure-driven changes to spontaneous flow in active nematic liquid crystals*, The European Physical Journal E, 43 (2020), pp. 1–14.
- [25] C. W. Wolgemuth, Collective swimming and the dynamics of bacterial turbulence, Biophysical Journal, 95 (2008), pp. 1564–1574.
- [26] S. Zhou, Recent progresses in lyotropic chromonic liquid crystal research: elasticity, viscosity, defect structures, and living liquid crystals, Liquid Crystals Today, 27 (2018), pp. 91–108.
- [27] S. Zhou, K. Neupane, Y. A. Nastishin, A. Baldwin, S. Shiyanovskii, O. Lavrentovich, and S. Sprunt, Elasticity, viscosity, and orientational fluctuations of a lyotropic chromonic nematic liquid crystal disodium cromoglycate, Soft matter, 10 34 (2014), pp. 6571–81.
- [28] S. Zhou, O. Tovkach, D. Golovaty, A. Sokolov, I. S. Aranson, and O. D. Lavrentovich, Dynamic states of swimming bacteria in a nematic liquid crystal cell with homeotropic alignment, New Journal of Physics, 19 (2017), p. 055006.